Journal of Hydrology 562 (2018) 609–622

Contents lists available at ScienceDirect

Journal of Hydrology

journal homepage: www.elsevier.com/locate/jhydrol

Research papers

A new model for simulating spring discharge recession and estimating effective porosity of karst aquifers

Bin Xu[a,b,c], Ming Ye[c,d,e,*], Shuning Dong[a,b,*], Zhenxue Dai[f], Yongzhen Pei[e]

[a] College of Geoscience and Surveying Engineering, China University of Mining and Technology, Beijing 100083, China
[b] China Coal Research Institute, Xi'an Research Institute, Xi'an 710054, China
[c] Department of Scientific Computing, Florida State University, Tallahassee, FL 32306, USA
[d] Department of Earth, Ocean, and Atmospheric Science, Florida State University, Tallahassee, United States
[e] School of Computer Science and Software Engineering, Tianjin Polytechnic University, Tianjin 300387, China
[f] College of Construction Engineering, Jilin University, Changchun 130026, China

ARTICLE INFO

This manuscript was handled by Corrado Corradini, Editor-in-Chief, with the assistance of Stephen Worthington, Associate Editor

Keywords:
Karst aquifer
Karst spring hydrograph
Recession curve
Hydrograph separation
Effective porosity
Conduit flow

ABSTRACT

Quantitative analysis of recession curves of karst spring hydrographs is a vital tool for understanding karst hydrology and inferring hydraulic properties of karst aquifers. This paper presents a new model for simulating karst spring recession curves. The new model has the following characteristics: (1) the model considers two separate but hydraulically connected reservoirs: matrix reservoir and conduit reservoir; (2) the model separates karst spring hydrograph recession into three stages: conduit-drainage stage, mixed-drainage stage (with both conduit drainage and matrix drainage), and matrix-drainage stage; and (3) in the mixed-drainage stage, the model uses multiple conduit layers to present different levels of conduit development. The new model outperforms the classical Mangin model and the recently developed Fiorillo model for simulating observed discharge at the Madison Blue Spring located in northern Florida. This is attributed to the latter two characteristics of the new model. Based on the new model, a method is developed for estimating effective porosity of the matrix and conduit reservoirs for the three drainage stages. The estimated porosity values are consistent with measured matrix porosity at the study site and with estimated conduit porosity reported in literature. The new model for simulating karst spring hydrograph recession is mathematically general, and can be applied to a wide range of karst spring hydrographs to understand groundwater flow in karst aquifers. The limitations of the model are discussed at the end of this paper.

1. Introduction

Quantitative analysis of the recession curves of karst spring hydrographs is a vital tool for various activities of water resources management in karst areas, such as calculating water budgets, estimating base flow rates, protecting aquatic ecosystems, and developing ecotourism resources under climate change (Fiorillo, 2009; Ghasemizadeh et al., 2012; Stevanovic, 2015). A recession curve, which is a falling limb after a peak on a spring hydrograph, can be viewed as an indicator of overall aquifer behaviors during a period without precipitation (Kiraly, 2003; Chang et al., 2015; Fu et al., 2016). Analyzing the recession curves helps characterize a karst aquifer, because hydrodynamic characteristics and hydraulic properties of the karst aquifer determine the shapes of recession curves (Bonacci, 1993; Dewandel et al., 2003; Fiorillo, 2011). For example, analysis of the recession curves is the basis for estimating effective aquifer porosity, and many methods have been developed in literature. The methods for estimating effective porosity can be categorized into direct methods (e.g., borehole drilling, speleological survey, cave diving, camera recording and logging, and remote-controlled vehicle) and indirect methods (e.g., tracing tests, geophysical survey, time series analysis, isotopic analysis, and spring hydrograph analysis) (Boussinesq, 1877, 1904; Maillet, 1905; Bonacci, 1993; Dewandel et al., 2003; Kovács, 2003; Kovács et al., 2005; Stevanovic et al., 2010; Fiorillo, 2011, 2014). Among these methods, the recession curves analysis has several advantages, such as being cost effective and providing large-scale aquifer properties and needing fewer parameters (Mangin, 1975; Bonacci, 1993; Dewandel et al., 2003; Kiraly, 2003; Kovács et al., 2005; Bailly-Comte et al., 2010; Ford and Williams, 2013; Chang et al., 2015; Goldscheider, 2015; Stevanovic, 2015). The choice of appropriate karst hydrogeology methods depends on the practical

* Corresponding authors at: Department of Earth, Ocean, and Atmospheric Science, Florida State University, Tallahassee, United States (M. Ye), China Coal Research Institute, Xi'an Research Institute, Xi'an 710054, China (S. Dong).
E-mail addresses: mye@fsu.edu (M. Ye), dongshng@sina.com (S. Dong).

https://doi.org/10.1016/j.jhydrol.2018.05.039
Received 26 December 2017; Received in revised form 15 May 2018; Accepted 16 May 2018
Available online 17 May 2018

and/or scientific research questions to be answered, the level of understanding of the system to be studied, and the amount of resources available (Goldscheider and Drew, 2007; Ford and Williams, 2013; Goldscheider, 2015).

This paper presents a new model for simulating the recession curves of karst spring hydrograph. The new model uses matrix and conduit reservoirs to represent a karst aquifer, which is a common feature of many models developed for karst spring hydrograph analysis (Martin and Dean, 2001; Martin and Screaton, 2001; Kiraly, 2003; Geyer et al., 2008; Shoemaker et al., 2008; Bailly-Comte et al., 2010; Ford and Williams, 2013; Chang et al., 2015). The new model is conceptually similar to the widely used Mangin model (Mangin, 1975) and the Fiorillo model (Fiorillo, 2011), but has its own features. The Mangin model uses two parallel reservoirs, a quick-flow reservoir for simulating discharge from unsaturated zones (e.g., conduits) and a slow-flow reservoir for simulating discharge from saturated zones (e.g., matrix). The Fiorillo model conceptualizes a karst aquifer as a series of tank reservoirs, i.e., the Torricelli reservoir for conduits, the Darcy reservoir for matrix, and the Poiseuille reservoir for fractures. Similar to the Mangin model, the new model of this study uses two reservoirs, i.e., a conduit reservoir and a matrix reservoir. The conduit reservoir is different from that of the Mangin model, but similar to the conduit reservoir of Fiorillo model. The matrix reservoir also differs from that of the Mangin model, and includes the matrix and fracture reservoirs of the Fiorillo model, because discharge from the matrix and fracture reservoirs can be simulated by two equations of the same form but with different physical meanings (Fiorillo, 2011).

Similar to the conceptualization of Taylor and Greene (2008), the new model of this study separates a karst spring hydrograph into three stages, the conduit-drainage stage (spring discharge from drainage (conduit flow) of conduit reservoir), the mixed-drainage stage (spring discharge from both drainage (conduit flow) of conduit reservoir and drainage (matrix flow) of matrix reservoir first to conduit reservoir and then to spring), and the matrix-drainage stage (spring discharge from drainage (matrix flow) of matrix reservoir first to conduit reservoir and then to spring). Using the three stages for hydrograph separation distinguishes the new model from the Mangin model, because the Mangin model considers that matrix flow contributes to spring discharge for the entire recession period whereas the new model does not consider matrix flow in the conduit-drainage stage of the recession period. The reason of not considering the matrix flow is that groundwater flows from conduits to matrix during the conduit-drainage stage, given that hydraulic head in the conduits is higher than the hydraulic head in the matrix. While the new model is similar to the Fiorillo model to separates a hydrograph into three stages, the new model differs from the Fiorillo model in that the new model has the mixed-drainage stage. The Fiorillo model does not use the concept of mixed drainage for the period between the conduit-drainage stage and the matrix-drainage stage. For this between-period, the Fiorillo model considers that the spring discharge is from well-connected fissures, and uses the Poiseuille reservoir to represent the fissures. The proposed mixed-drainage stage is consistent with the observation that water level in conduits continues decreasing in the period between the conduit-drainage stage and the matrix-drainage stage, which indicates that conduit flow exists in the period (Shevenell, 1996; Taylor and Greene, 2008). If conduit flow is negligible during the mixed-drainage stage, the mixed flow becomes the matrix flow only (or the flow from the Poiseuille reservoir in the Fiorillo model). As shown in Section 4 below, due to using the mixed-drainage concept and enabling the flexibility of multiple conduit layers, the results of the new model are better than those of the current implementation of the Fiorillo model for simulating the observed discharge at the Madison Blue Spring located in northern Florida.

The new model of karst spring hydrograph analysis provides a basis for estimating groundwater flow from matrix and conduit reservoirs separately and for estimating effective porosity of matrix and conduit reservoirs separately. Estimating matrix and conduit drainage separately helps understand the relative significance of conduit drainage and matrix drainage in a recession period. Since effective porosity is an important aquifer property for managing water resources of karst areas (Fu et al., 2016), many methods have been developed to estimate effective porosity of karst aquifers (Boussinesq, 1904; Bonacci, 1993; Shevenell, 1996; Szilagyi, 1999; Dewandel et al., 2003; Kovács et al., 2005; Fiorillo, 2011, 2014). However, these methods consider a karst aquifer as a whole, and do not separate matrix flow and conduit flow. Therefore, the existing methods cannot estimate effective porosity of conduit and matrix reservoir separately, which may limit our understanding of karst aquifers. This problem is resolved in this study by separating matrix flow and conduit flow. In addition, multiple conduit layers are used to represent different levels of conduit development, and the effective porosity of each conduit layer is estimated. Estimating effective matrix and conduit porosity for the three drainage stages enables us to better characterize the karst aquifer for the entire recession period.

The rest of the paper is organized as follows. The new model for simulating recession curves of karst spring hydrograph, the method of estimating conduit and matrix flows, and the method of estimating effective porosity of matrix and conduit reservoirs are discussed in Section 2. The new model was used for simulating observed spring discharge at the Madison Blue Spring, and the field site and observations of hydraulic head and discharge are described in Section 3. Two recession periods with different hydrological and groundwater conditions are chosen for evaluating the simulations given by the three models, i.e., the new model of this study, the Mangin model, and the Fiorillo model. The simulation results and the evaluation of the three models are given in Section 4. This section also discusses the results of estimating matrix and conduit drainage as well as effective porosity of matrix and conduit reservoirs. The major conclusions of this research are given in Section 5.

2. Methodology

This section starts with a detailed description of the new model of karst spring hydrograph analysis in Section 2.1. Section 2.2 includes a brief description of the Mangin model and the Fiorillo model that are compared with the new model in this study. The method of estimating matrix and conduit flows and the method of estimating effective porosity of matrix and conduit reservoirs are described in Section 2.3.

2.1. New model of simulating recession curves of karst spring hydrograph

The new model of simulating the recession curves of karst spring hydrograph has the following characteristics:

(1) The matrix and conduits of a karst aquifer are considered as two separate reservoirs. This conceptualization of karst aquifer has been widely used for simulating karst spring hydrograph.
(2) A recession period on a karst spring hydrograph is separated into three stages: conduit-drainage stage (Stage I), mixed-drainage stage (Stage II), and matrix-drainage stage (Stage III), as shown in Fig. 1. During the mixed-drainage stage, the conduit flow (in conduits) and matrix flow (from matrix to conduits) are separated explicitly in the new model.
(3) In the mixed-drainage stage, multiple conduit layers are used to represent different levels of conduit development (Fig. 1). Note that the conduit layers are different from the tanks of the Fiorillo model that includes both conduits and matrix.

Explicitly separating matrix and conduit flows and using multiple conduit layers for representing different levels of karst development are two unique features of the new model for simulating spring discharge of the recession periods of karst spring hydrograph.Fig. 2 illustrates the three characteristics discussed above and the conceptual model of the

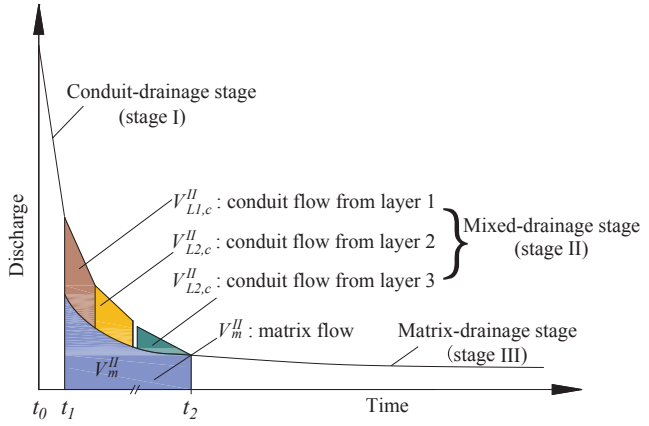

Fig. 1. Three stages used in the recession spring hydrograph analysis: conduit-drainage stage (Stage I), mixed-drainage stage (Stage II), and matrix-drainage stage (Stage III). In the mixed-drainage stage, spring discharge consists of matrix flow and conduit flow from multiple conduit layers.

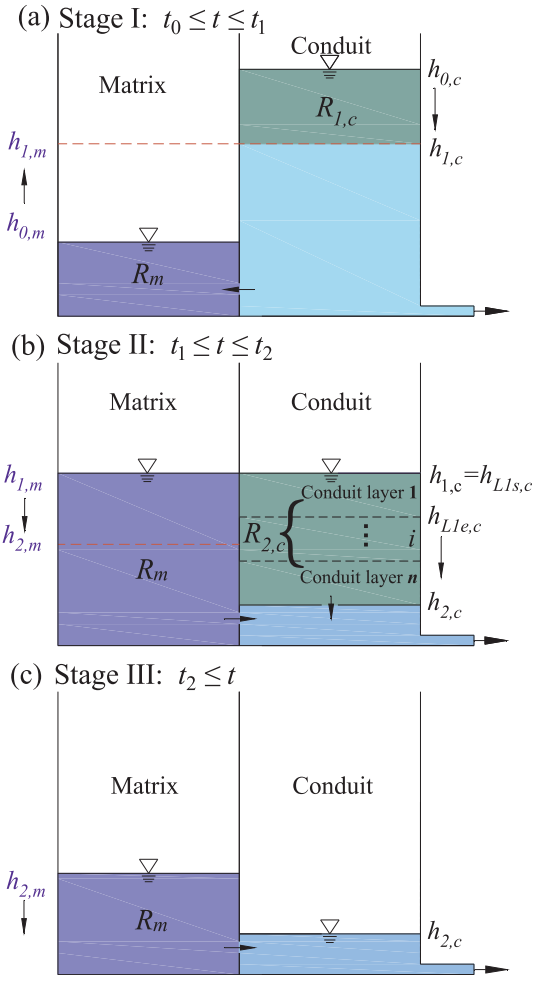

Fig. 2. Sketch of the dynamics of conduit flow and matrix flow in the three stages of the new model. The conduit-drainage stage (Stage I) ends when hydraulic head in the conduit reservoir decreases from $h_{0,c}$ to $h_{1,c}$ (from t_0 to t_1) and when hydraulic head in the matrix reservoir increases from $h_{0,m}$ to $h_{1,m}$, which equals to $h_{1,c}$. The mixed-drainage stage (Stage II) ends when hydraulic head in the conduit reservoir decreases from $h_{1,c}$ to $h_{2,c}$ (from t_1 to t_2) and when hydraulic head in the matrix reservoir decreases from $h_{1,m}$ to $h_{2,m}$. In the matrix-drainage stage (Stage III), hydraulic head in the conduit reservoir remains at $h_{2,c}$, and hydraulic head in the matrix reservoir continues decreasing from $h_{2,m}$ until the next rainfall event.

dynamics of matrix and conduit flows for understanding karst spring hydrograph recession. During the conduit-drainage stage (Stage I) (Fig. 2a), conduit flow is the only source of spring discharge, and hydraulic head in the conduit reservoir decreases from $h_{0,c}$ to $h_{1,c}$ (from t_0 to t_1). The spring discharge, Q_t^I [L^3T^{-1}], of the conduit-drainage stage for time $t_0 \le t \le t_1$ can be evaluated using the equations below derived by following (Fiorillo, 2011). Based on the conceptualization of Torricelli reservoir of Fiorillo (2011), the spring discharge, Q_t^I, is expressed as

$$Q_t^I = A_{2,c}\sqrt{2gh_{t,c}}, \tag{1}$$

where $A_{2,c}$ is the area of spring outlet [L^2], g is the gravity acceleration [LT^{-2}], and $h_{t,c}$ is hydraulic head of the conduit reservoir [L]. Based on the principle of mass balance that the variation rate of water storage in the conduit reservoir equals to the spring discharge during the hydrograph recession, we have the differential equation of $h_{t,c}$ as (Bailly-Comte et al., 2010; Fiorillo, 2011):

$$A_{1,c}\frac{dh_{t,c}}{dt} = -Q_t^I = -A_{2,c}\sqrt{2gh_{t,c}}, \tag{2}$$

where $A_{1,c}$ is the horizontal area of the conduit reservoir [L^2]. Integrating Eq. (2) for time t_0 to t_1 and for the hydraulic head from $h_{0,c}$ to $h_{1,c}$ gives (Fiorillo, 2011)

$$2\sqrt{h_{t,c}} - 2\sqrt{h_{0,c}} = -\frac{A_{2,c}}{A_{1,c}}\sqrt{2g}\,t. \tag{3}$$

Substituting Eq. (1) into Eq. (3) gives (Kullman, 1990; Fiorillo, 2011):

$$Q_t^I = Q_0^I - \gamma t, \tag{4}$$

for $t_0 \le t \le t_1$, where $Q_0^I = A_{2,c}\sqrt{2gh_{0,c}}$ is the initial spring discharge at time $t = 0$ [L^3T^{-1}], and $\gamma = \frac{A_{2,c}^2}{A_{1,c}}g$ is the recession coefficient of the conduit reservoir [L^3T^{-2}]. To use Eq. (4) for simulating karst spring discharge requires estimating Q_0 and γ based on field measurements of spring discharge. When estimating γ from discharge measurements, the two areas, $A_{1,c}$ and $A_{2,c}$, are not needed for using Eq. (4).

In the conduit-drainage stage (Stage I), hydraulic head in the matrix increases from $h_{0,m}$ to $h_{1,m}$ (Fig. 2a) due to infiltration of rainfall into the matrix. The discharge of conduit flow to the matrix is considered to be negligible, according to Peterson and Wicks (2005), who found that the volume of fluid penetrating from flooded conduits into the matrix is less than 1% of the volume of fluid flowing in the conduits. While the finding of Peterson and Wicks (2005) may not be the case for the Floridan aquifer with relatively large secondary porosity, the ignorance of the discharge of conduit flow into matrix appears to be valid in the field application of the new model, as described below. Exploring the influence of the discharge volume (i.e., bank storage) on the recession mechanism and the recession curve is warranted in a future study.

When the hydraulic head in the conduit reservoir decreases from $h_{0,c}$ to $h_{1,c}$ (from t_0 to t_1) and when the hydraulic head in matrix reservoir increases from $h_{0,m}$ to $h_{1,m}$ (from t_0 to t_1) that equals to $h_{1,c}$, the mixed-drainage stage (Stage II) starts (Fig. 2b). During this stage, the hydraulic head in the conduit reservoir continues decreasing from $h_{1,c}$ to $h_{2,c}$ (from t_1 to t_2), and the hydraulic head in the matrix reservoir starts decreasing, from $h_{1,m}$ to $h_{2,m}$ (from t_1 to t_2). Since the head decreases in the conduit reservoir is faster than that in the matrix reservoir, groundwater discharges from the matrix to conduits, and the spring discharge is composed of both conduit flow and matrix flow. Although the exchange mechanism between the conduit reservoir and the matrix reservoir is complicated, it is reasonable to assume that matrix flow and conduit flow are independent, i.e., the matrix flow do not affect the conduit flow and vice versa (Peterson and Wicks, 2005; Malík and Vojtková, 2012; Li and Field, 2013; Li et al., 2016). Following the assumption, the matrix flow and conduit flow are simulated separately. The matrix flow for time period $t_1 \le t \le t_2$ can be evaluated

via (Maillet, 1905; Kovács et al., 2005)

$$Q_{t,m}^{II} = Q_{1,m} e^{-\alpha_1 (t-t_1)}, \quad (5)$$

where $Q_{t,m}^{II}$ is the discharge rate of the matrix reservoir [L^3T^{-1}], $Q_{1,m}$ is the starting matrix discharge at time $t = t_1$ when $h_{1,m} = h_{1,c}$ [L^3T^{-1}], and α_1 [T^{-1}] is the recession coefficient of the matrix reservoir during the mixed-drainage stage. The parameters, $Q_{1,m}$ and α_1, are estimated from field measurements of spring discharge, as described below.

Fiorillo (2011) derived Eq. (5) for Darcy reservoir of porous media and for Poiseuille reservoir of fractured media. Since Eq. (5) can be used for evaluating both matrix flow and fracture flow, the new model of this study does not distinguish matrix and fracture reservoirs, but calls both of them as matrix reservoir. Note that Eq. (5) is not used for simulating the recession curve in the conduit-drainage stage.

For the conduit flow in the mixed-drainage stage (Stage II), the new model uses multiple conduit layers to represent different levels of karstification in depth (Fig. 2b). For the i-th conduit layer (denoted as Li), similar to the derivation of Eq. (4), the discharge rate for $t_{Lis,c} \le t \le t_{Lie,c}$ ($t_{Lis,c}$ and $t_{Lie,c}$ being the starting and ending times of groundwater drainage from conduit layer Li, respectively) is derived as

$$Q_{t,Li,c}^{II} = Q_{Lis,c} - \beta_i (t - t_{Lis,c}), \quad (6)$$

where $Q_{t,Li,c}^{II}$ is the discharge rate of the i-th conduit layer [L^3T^{-1}], $Q_{Lis,c}$ is the starting discharge from the i-th conduit layer [L^3T^{-1}], β_i is the recession coefficient for the i-th conduit layer [L^3T^{-2}], $t_{Lis,c}$ is the starting time of the discharge from the i-th conduit layer [T]. In this study, coefficients, $Q_{Lis,c}$, β_i, and $t_{Li,c}$, of Eq. (6) are estimated from field measurements of spring discharge, as described below.

Combining Eqs. (5) and (6) gives the spring discharge from the i-th conduit layer and the matrix reservoir as

$$Q_{t,Li}^{II} = Q_{t,Li,c}^{II} + Q_{t,m}^{II} = (Q_{Lis,c} - \beta_i (t - t_{Lis,c})) + Q_{1,m} e^{-\alpha_1 (t-t_1)}. \quad (7)$$

during the mixed-drainage stage (stage II). The total spring discharge from the matrix reservoir and all the conduit layers is

$$Q_{t,Li}^{II} = \sum_i Q_{t,Li,c}^{II} + Q_{t,m}^{II} = \sum_i (Q_{Lis,c} - \beta_i (t - t_{Lis,c})) + Q_{1,m} e^{-\alpha_1 (t-t_1)}. \quad (8)$$

For an aquifer with a high level of karstification, the matrix flow may be negligible. When the conduit flow is negligible, our model is similar to the Mangin model and the Fiorillo model, in that the spring discharge is controlled mainly by the matrix flow. When the conduit flow is not negligible and both matrix flow and conduit are important, our model is expected to provide better simulation to measured spring discharge than the Mangin model and the Fiorillo model do, which is demonstrated in the real-world application in Section 4.

The relative importance of matrix flow and conduit flow depends on the level of karstification, as different levels of karstification result in the vertical variation of hydraulic conductivity and porosity (Milanovic, 1981; Kullman, 1990; Fiorillo, 2011). Based on hydrograph recession analyses of nine-gauged springs located in a Slovak aquifer, Malík and Vojtková (2012) provided the link between recessional equations and a total of ten karstification degrees defined by the authors. The recessional equations only include matrix flow for karstification degree less than four, the recessional equations include both matrix flow and conduit flow for karstification degree between four and eight, and the recessional equations include only conduit flow for karstification degree larger than eight. It however should be noted that the definitions of the karstification levels are site-specific, and they should be used for other karst aquifers with cautions.As shown in Fig. 2c, the matrix-drainage stage (Stage III) starts when the hydraulic head in the conduit reservoir decreases from $h_{1,c}$ to $h_{2,c}$ at time $t = t_2$ and stabilizes at $h_{2,c}$; meanwhile the hydraulic head in the matrix reservoir continues decreasing from $h_{2,m}$ until the next rainfall event. In this stage, the recession curve of karst spring hydrograph is mainly controlled by the baseflow from the matrix reservoir. According to Kovács et al. (2005), the hydraulic head, $h_{2,c}$, acts as the fixed head boundary when spring discharge is mainly controlled by the matrix reservoir, because the conduit network has no influence on the spring discharge and negligible storage in the conduit reservoir contributes to spring discharge. Following the literature (Maillet, 1905; Kovács et al., 2005; Bailly-Comte et al., 2010; Malík and Vojtková, 2012; Goldscheider, 2015), the matrix flow, Q_t^{III} [L^3T^{-1}], is evaluated via

$$Q_t^{III} = Q_{2,m} e^{-\alpha_2 (t-t_2)} \quad (9)$$

where $Q_{2,m}$ is the discharge rate of the matrix reservoir at time $t = t_2$ [L^3T^{-1}], and α_2 is the recession coefficient of the matrix reservoir [T^{-1}]. Using Eq. (9) for simulating the spring hydrograph requires estimating $Q_{2,m}$ and α_2 based on field measurements of spring discharge.

The procedure of using the equations above to simulate karst spring hydrograph is as follows:

(1). Separate a karst spring hydrograph into the three stages (conduit-drainage, mixed-drainage, and matrix-drainage) in two steps. The first step is to determine time t_1, the end of the conduit-drainage stage (Stage I). Since the flow rate of this stage is a linear function of time (Eq. (4)), t_1 is determined as the time when the linear hydrograph ends. The second step is to determine time t_2, the beginning of the matrix-drainage stage (Stage III), by first plotting the logarithm of the hydrograph with time. Time, t_2, is selected as the beginning of linear semi-log plot with respect to time, because the semi-log plot is a straight line with time (Eq. (9)). After t_1 and t_2 are determined, the karst spring hydrograph is separated into the conduit-drainage stage, mixed-drainage stage, and matrix-drainage stage.

(2). For the conduit-drainage stage (Stage I), by fitting Eq. (4) to discharge measurements to estimate Q_0^I and γ.

(3). Simulation the matrix-drainage stage (Stage III) by fitting Eq. (9) to discharge measurements to estimate $Q_{2,m}$ and α_2.

(4). Simulate the matrix flow of the mixed-drainage stage (Stage II) by using Eq. (5), which requires estimating parameters α_1 and $Q_{1,m}$ of the equation. Assuming that the matrix reservoir behaves in the same way for producing matrix flow in the matrix-flow and mixed-drainage stages, assign the value of α_2 estimated above to α_1, which is also used in literature (Mangin, 1975; Kovács et al., 2005; Kovács and Perrochet, 2008). To estimate $Q_{1,m}$, because the matrix flow of the mixed-drainage stage equals to the matrix flow of the matrix-drainage stage at $t = t_2$, we set $Q_{t,m}^{II} = Q_{1,m} e^{-\alpha_2 (t_2 - t_1)} = Q_{2,m}$ based on Eqs. (5) and (9). This leads to $Q_{1,m}$ directly.

(5). Simulate the conduit flow of the mixed-drainage stage (Stage II) by subtracting the simulated matrix flow in Step (4) above from the discharge measurements. This results in the conduit flow from all conduit layers, according to Eq. (8). Since the conduit flow of each conduit layer is a linear function of time (Eq. (6)), the hydrograph of the conduit flow can be separated into multiple linear segments to determine $t_{Lis,c}$, the start time of the discharge from the i-th conduit layer (denoted as Li). Afterward, $Q_{Lis,c}$ and β_i of Eq. (6) can be estimated by fitting the equation to corresponding measurements of spring discharge. The number of conduit layers is determined empirically for achieving satisfactory fit to measured spring discharge. The real-world application of the new model below shows that using two conduit layers achieves significantly better fit than using one conduit layer.

The curve fitting operations above is carried out manually, and automatic curve-fitting can be done using regression techniques (Draper and Smith, 1998).

2.2. Comparison with two other models

The new model of this study is compared with two widely used models: the Mangin model and the Fiorillo model. As shown in Fig. 3a, the Mangin model does not separate a karst aquifer into matrix and

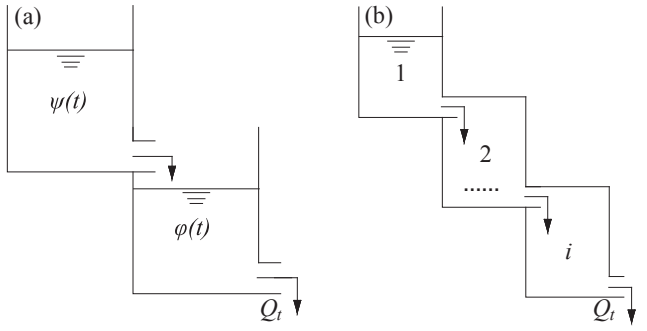

Fig. 3. Diagrams of (a) Mangin model and (b) Fiorillo tank model.

conduit reservoirs. Instead, the model consists of a reservoir of saturated zone (e.g., conduits) and a reservoir of unsaturated zone (e.g., matrix). The spring discharge from the two reservoirs is calculated via (Mangin, 1975)

$$Q_t = \psi(t) + \varphi(t) = Q_q \frac{1-\eta t}{1+\varepsilon t} + Q_b e^{-\alpha_b t} \tag{10}$$

where $\psi(t)$ is the discharge from unsaturated zone [L^3T^{-1}], $\varphi(t)$ is the discharge from saturated zone [L^3T^{-1}], Q_q is the maximal infiltration flowrate [L^3T^{-1}], η [T^{-1}] is the inverse of the period of infiltration, ε is the concavity of the recession curve resulting from infiltration heterogeneity, Q_b is the initial saturated flow rate [L^3T^{-1}], and α_b is a recession coefficient [T^{-1}]. All the coefficients (Q_q, η, ε, Q_b, and α_b) are estimated based on measurements of spring discharge. More details of the Mangin model and its application are referred to literature (Mangin, 1975; Dewandel et al., 2003; Ford and Williams, 2013; Fu et al., 2016).

As shown in Fig. 3b, the Fiorillo model considers a series of tank reservoirs. The first reservoir (denoted as 01 in Fig. 3b) is the Torricelli tank reservoir that represents drainage from shafts and upper conduits, and its flow rate is estimated as (Fiorillo, 2011)

$$Q_t = Q_{0,1} - \alpha_T t, \tag{11}$$

where $Q_{0,1}$ is the initial discharge of the Torricelli tank reservoir, and α_T is the recession coefficients of the reservoir [T^{-1}]. Other reservoirs are the Darcy and Poiseuille reservoirs, and their discharges are estimated as (Fiorillo, 2011)

$$Q_{t,i} = Q_{0,i} e^{-\alpha_i t}, \tag{12}$$

where $Q_{0,i}$ [L^3T^{-1}] is the initial discharge of the i-th reservoir, and α_i [T^{-1}] is the recession coefficient of the i-th reservoir. All the coefficients ($Q_{0,1}$, α_T, $Q_{0,i}$, and α_i) are estimated based on measurements of spring discharge. More details of the Fiorillo model and its application are referred to Fiorillo (2011).

To compare the new model of this study with the two models above, the three models are used to simulate real-world measurements of the discharge of the Madison Blue Spring located in northern Florida, and the misfit between simulated and measured discharge is used as the criterion for evaluating the model performance. The misfit is calculated as

$$\text{misfit} = \sum_{i=1}^{n} |r_i| \tag{13}$$

where r_i is the residual between simulated and measured discharge.

2.3. Estimation of discharge volume and effective porosity

Based on the hydrograph modeling above, we can estimate the discharge volumes from the matrix and conduit reservoirs, which in turn can be used to estimate effective porosity of the matrix and conduit reservoirs. This section starts with the estimations for the mixed-drainage stage (Stage II), and then discusses the estimations for the other two drainage stages. Fig. 1 illustrates the separation of matrix discharge and conduit discharge for the mixed-drainage stage; the conduit discharge is further separated to the discharge from each conduit layer. These make it possible to explicitly estimate the effective porosity of the matrix reservoir and the effective porosity of individual conduit layers.For the mixed-drainage stage, the effective porosity of the matrix reservoir, n_m^{II}, is defined as the volume of water discharged from the matrix reservoir when hydraulic head of the matrix reservoir decreases from $h_{1,m}$ to $h_{2,m}$ (i.e., from time t_1 to time t_2 shown in Fig. 2b and estimated in Step (1) of Section 2.1 above), i.e.,

$$n_m^{II} = \frac{V_m^{II}}{(h_{1,m} - h_{2,m}) A_c} \tag{14}$$

where V_m^{II} is the groundwater discharge from the matrix reservoir during the mixed-drainage stage (Stage II), and A_c is the drainage area of the karst aquifer. While A_c is always available for a groundwater basin, $h_{1,m}$, $h_{2,m}$, and V_m^{II} need to be estimated. Since $h_{1,m}$ and $h_{2,m}$ are the average hydraulic head of the matrix reservoir, the isoline method described in Gupta (2016) is used for estimating the average heads. In the isoline method, contours of the hydraulic head are first generated using measurements of hydraulic head, and the weighted average of hydraulic head, h, is evaluated via

$$h = \sum_{i=1}^{n} A_i \frac{(h_{i-1} + h_i)}{2} \Big/ \sum_{i=1}^{n} A_i, \tag{15}$$

where h_{i-1} and h_i are the values of the hydraulic head for a pair of isoclines, and A_i is the area between the pair of isolines. The areas are used as the weights for estimating the average hydraulic head of the matrix reservoir. After a time series of the average head is obtained based on head measurements, $h_{1,m}$ for time t_1 and $h_{2,m}$ for time t_2 can be approximated. The volume of groundwater discharge, V_m^{II}, from the matrix reservoir is estimated by integrating the matrix flow (Eq. (5)) from t_1 to t_2 as

$$V_m^{II} = \int_{t_1}^{t_2} Q_{t,m}^{II} dt = \int_{t_1}^{t_2} Q_{1,m} e^{-\alpha_1 (t-t_1)} dt = \frac{Q_{1,m} - Q_{2,m}}{\alpha_1}, \tag{16}$$

where $Q_{1,m}$ is estimated in Step (4), and $Q_{2,m}$ and α_1 are estimated in Step (3) of Section 2.1 above.For the mixed-drainage stage, the effective porosity of the conduit reservoir, n_c^{II}, is defined as the volume of water discharged from the conduit reservoir when hydraulic head of the conduit reservoir decreases from $h_{1,c}$ and $h_{2,c}$ (i.e., from time t_1 to time t_2 shown in Fig. 2b and estimated in Step (1) of Section 2.1 above). The effective porosity, $n_{Li,c}^{II}$, of the i-th conduit layer (denoted as Li) is defined as

$$n_{Li,c}^{II} = \frac{V_{Li,c}^{II}}{(h_{Lis,c} - h_{Lie,c}) A_c}, \tag{17}$$

where $V_{Li,c}^{II}$ is the volume of groundwater discharged from the i-th conduit layer, and $h_{Lis,c}$ and $h_{Lie,c}$ are the starting and ending hydraulic heads when groundwater discharges from the i-th conduit layer. $h_{Lis,c}$ and $h_{Lie,c}$ correspond to $t_{Lis,c}$ and $t_{Lie,c}$ (used in Eq. (6)), respectively, and the starting and ending discharge times ($t_{Lis,c}$ and $t_{Lie,c}$) are obtained in Step (5) of Section 2.1 above. The discharge volume, $V_{Li,c}^{II}$, is estimated by integrating the conduit flow (Eq. (6)) from t_{Lis} to t_{Lie} (the starting and ending times, respectively, when groundwater discharges from the i-th conduit layer) as

$$V_{Li,c}^{II} = \int_{t_{Lis,c}}^{t_{Lie,c}} Q_{t,Li,c}^{II} dt = \int_{t_{Lis,c}}^{t_{Lie,c}} (Q_{Lis,c} - \beta_i (t - t_{Lis,c}))dt$$
$$= \left[Q_{Lis,c}(t - t_{Lis,c}) - \frac{1}{2}\beta_i (t - t_{Lis,c})^2 \right] \Big|_{t_{Lis,c}}^{t_{Lie,c}}$$
$$= -\frac{Q_{Lis,c}^2 - 2Q_{Lis,c}\beta_i (t_{Lie,c} - t_{Lis,c}) + (\beta_i (t_{Lie,c} - t_{Lis,c}))^2}{2\beta_i}$$
$$+ \frac{Q_{Lis,c}^2 - 2Q_{Lis,c}\beta_i (t_{Lis,c} - t_{Lis,c}) + (\beta_i (t_{Lis,c} - t_{Lis,c}))^2}{2\beta_i}$$
$$= -\frac{(Q_{Lis,c} - \beta_i (t_{Lie,c} - t_{Lis,c}))^2}{2\beta_i} + \frac{(Q_{Lis,c} - \beta_i (t_{Lis,c} - t_{Lis,c}))^2}{2\beta_i}$$
$$= \frac{Q_{Lis,c}^2 - Q_{Lie,c}^2}{2\beta_i}. \quad (18)$$

where $Q_{Lis,c}$, $Q_{Lie,c}$, and β_i are estimated in Step (5) of Section 2.1 above.

Since there is no measurement of conduit head, the isoline method above cannot be used for estimating average conduit head (e.g., $h_{Lis,c}$ and $h_{Lie,c}$), which is a theoretical weakness of the new model as conduit heads are rarely available in practice. To address this problem, this study estimates hydraulic head of each conduit layer by linking conduit head with conduit discharge. The estimation starts from $h_{L1s,c}$ and $h_{L1e,c}$, the starting and ending hydraulic heads when groundwater discharges from the first conduit layer. As shown in Fig. 2b, for the starting hydraulic head, we have $h_{L1s,c} = h_{1,c} = h_{1,m}$. For estimating the ending hydraulic head, $h_{L1e,c}$, we relate the hydraulic head with the conduit discharge at the beginning and the ending time of the discharge period, which are denoted as $Q_{L1s,c}$ and $Q_{L1e,c}$ respectively. By virtue of Eq. (1), we have

$$Q_{L1s,c} \propto \sqrt{2g(h_{L1s,c} - h_{2,c})}\, Q_{L1e,c} \propto \sqrt{2g(h_{L1e,c} - h_{2,c})}. \quad (19)$$

Taking the ratio between $Q_{L1e,c}$ and $Q_{L1s,c}$ leads to

$$\frac{Q_{L1e,c}}{Q_{L1s,c}} = \sqrt{\frac{h_{L1e,c} - h_{2,c}}{h_{L1s,c} - h_{2,c}}}. \quad (20)$$

Rearranging the equation gives

$$h_{L1e,c} = (h_{L1s,c} - h_{2,c})\left(\frac{Q_{L1e,c}}{Q_{L1s,c}}\right)^2 + h_{2,c} \quad (21)$$

Considering $h_{L1s,c} = h_{1,m}$, $Q_{L1s,c} = Q_{t,L1,c}^{II}$, and $Q_{L1e,c} = Q_{t,L2,c}^{II}$, Eq. (21) becomes

$$h_{L1e,c} = (h_{1,m} - h_{2,c})\left(\frac{Q_{t,L1,c}^{II}}{Q_{t,L2,c}^{II}}\right)^2 + h_{2,c}. \quad (22)$$

This equation can be readily evaluated, because $h_{1,m}$ is estimated using Eq. (15) and in addition $Q_{t,L1,c}^{II}$ and $Q_{t,L2,c}^{II}$ are estimated in Step (5) of Section 2.1 above. For the i-th conduit layer beneath the first layer, Eq. (21) becomes

$$h_{Lie,c} = (h_{Lis,c} - h_{2,c})\left(\frac{Q_{t,Li,c}^{II}}{Q_{t,Li+1,c}^{II}}\right)^2 + h_{2,c} \quad (23)$$

where $h_{Lis,c} = h_{Li-1e,c}$ (i.e., the starting head of the i-th conduit layer is the ending head of the (i-1)-th conduit layer). For the bottom conduit layer, $h_{Lie,c} = h_{2,c}$, the average hydraulic head in the conduit reservoir at t_2 (Fig. 2c). Estimating $h_{2,c}$ is more difficult than estimating $h_{2,m}$, because measurements of hydraulic head in conduit reservoir are always lacking. An assumed value may be assigned to $h_{2,c}$ based on measurements of river stage and/or matrix hydraulic head. The impacts of assumed $h_{2,c}$ on the estimation of effective porosity of conduit layers are discussed in Section 4 of the real-world application of the new method of hydrograph modeling.The above estimation of effective porosity for the mixed-drainage stage can be applied directly to the conduit-flow and matrix-drainage stages. For the conduit-drainage stage, similar to Eq. (17), the effective porosity, n_c^I, of conduit reservoir is defined as

$$n_c^I = \frac{V_c^I}{(h_{0,c} - h_{1,c})A_c}, \quad (24)$$

where V_c^I is the volume of groundwater discharged from the conduit reservoir when conduit head decreases from $h_{0,c}$ to $h_{1,c}$ from time t_0 to time t_1 (i.e., the duration of Stage I shown in Fig. 2a). The discharge volume, V_c^I, can be estimated by integrating conduit flow, Q_t^I (Eq. (4)), from t_0 to t_1, which, similar to Eq. (18), leads to

$$V^I = \frac{(Q_0^I)^2 - (Q_1^I)^2}{2\gamma}. \quad (25)$$

In this equation, Q_0^I and γ are estimated in Step (2) of Section 2.1 above, and Q_1^I (the discharge at t_1) can be calculated using Eq. (4). The conduit hydraulic head $h_{1,c}$ in Eq. (4) takes the value of $h_{1,m}$ as discussed above, and $h_{0,c}$ in Eq. (24) needs to be estimated indirectly, due to the lacking of conduit head data. Following the derivation of Eqs. (19)–(23), the expression of $h_{0,c}$ is derived as

$$h_{0,c} = h_{1,c}\left(\frac{Q_0^I}{Q_1^I}\right)^2 \quad (26)$$

The effective porosity, n_m^{III}, of the matrix reservoir for the matrix-drainage stage is defined as

$$n_m^{III} = \frac{V_m^{III}}{h_{2,m} - h_{3,m}} \quad (27)$$

where V_m^{III} is the amount of groundwater discharge from the matrix reservoir. It can be estimated by integrating the matrix flow, Q_t^{III} (Eq. (9)), from t_2 to t_3, which, similar to Eq. (16) gives

$$V^{III} = \int t_2^{t_3} Q_{t,m}^{III} dt = \frac{Q_{2,m} - Q_{3,m}}{\alpha_1}. \quad (28)$$

In this equation, $Q_{2,m}$ and α_1 are estimated in Step (3) of Section 2.1 above, and $Q_{3,m}$ can be estimated by using Eq. (9). The matrix heads, $h_{2,m}$ and $h_{3,m}$, can be obtained from the average matrix head (Eq. (15)) discussed above.

3. Study area and field data

Fig. 4 shows the location of the study area in the Madison County, Florida. The Madison Blue Spring (shown in the insertion) is a first magnitude spring, and the spring vent (latitude 30°28′49″ and longitude 83°14′40″) is located on the eastern border of Madison County adjacent to the Withlacoochee River. The spring vent is connected to an unconfined aquifer by a network of phreatic conduits in the Suwannee Limestone and the underlying Ocala Limestone. The land surface altitude of the spring is 14.63 m above NGVD29 (USGS, 2017). The spring discharge ranges from 2 to 4 m^3/s, and the average discharge over the period of 2002–2017 is 2.8 m^3/s (USGS, 2017). The annual average precipitation is 1335 mm (NOAA, 2017). The average annual recharge from precipitation to the karst aquifer is approximately 254 mm (Copeland, 2003). The wet season is June–September, and the dry season is October–May. The area of the springshed is estimated to be 259 km^2 (Greenhalgh, 2003; SRWMD, 2004a, b), and it is used in Eqs. (14) and (17) for estimating the effective porosity of matrix and conduit layers.

The aquifer system in the study area consists of (from top to bottom) a surficial aquifer, an intermediate aquifer, a confining unit, and the Floridan aquifer System (Scott, 1988). Despite of the existence of the confining unit, the entire aquifer system is considered to be poorly confined for two reasons. First, since the siliciclastic and carbonate horizons in the intermediate aquifer and the confining unit are permeable, the intermediate aquifer and the confining unit act as a semi-confining unit that separates the surficial aquifer and the Floridan aquifer. In addition, because of sinkholes and eroded zones in the intermediate aquifer and confining unit, the Floridan aquifer is poorly confined, and recharge to the Florida aquifer is relatively effective

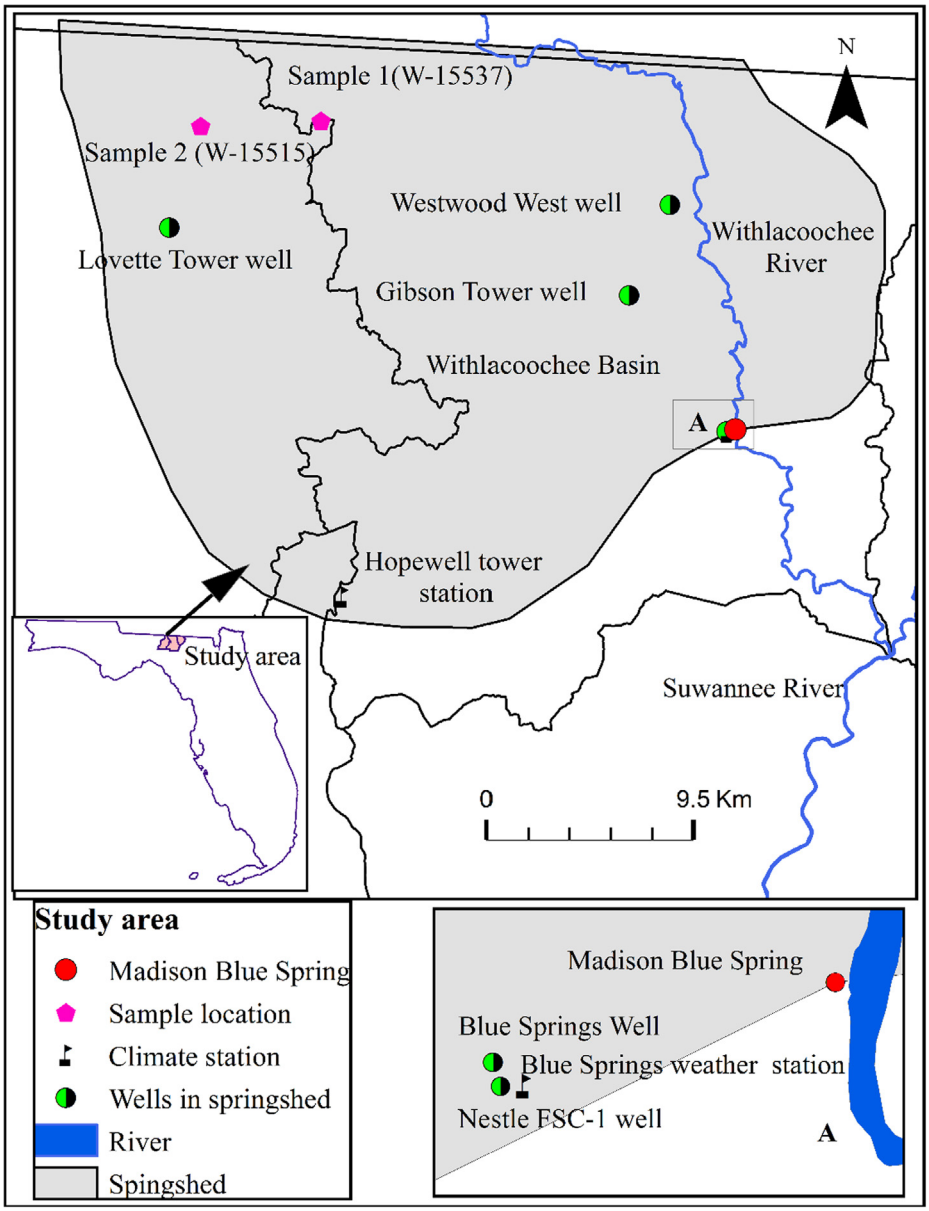

Fig. 4. Location map of the study area (SRWMD 2017a,b; USGS 2017). The springshed delineation is .** adopted from Greenhalgh (2003)

throughout the springshed (Bush and Johnston, 1988; Grubbs, 1998; Arthur et al., 2005). Therefore, it is suitable to apply the new model to analyze the karst spring hydrograph of the Madison Blue Spring.

Fig. 5 plots the time series of daily precipitation, spring discharge, and hydraulic head for the period from October 6, 2012 to June 6, 2017. The spring discharge is monitored at the Madison Blue Spring station by the U.S. Geological and Survey (USGS) (USGS, 2017). Daily precipitation is monitored at the Madison Blue Springs weather station and Hopewell Tower station (Fig. 4) by the Suwannee River Water Management District (SRWMD, 2017a). The average precipitation of the two stations is plotted in Fig. 5. A groundwater monitoring network has been established in this area by USGS and the water management district. The daily hydraulic head is recorded at five monitoring wells: Blue Spring, Nestle FSC-1, Gibson Tower, Westwood West, and Lovette Tower (SRWMD, 2017b). All the wells were drilled into the Floridan aquifer, and fractures and small karst conduits were encountered during drilling. For the convenience of hydrograph analysis, a reference head ($h = 0$ m) is set at $h = 12.4$ m (above NGVD29), which is the base-flow spring water level (USGS, 2017; SRWMD, 2017b). The hydraulic head at the Blue Spring well and Nestle FSC-1 well are almost identical, and overlap together in Fig. 5.

Fig. 5 shows that the spring discharge and hydraulic head respond quickly to rainfall events, in that the discharge and hydraulic head increase immediately after rainfalls. It is noted that, after hydraulic heads reach the peak values, the spring discharge becomes smaller and sometimes becomes negative. This is due to backflow of stream water into the spring vent, because the water level of the Withlacoochee River increases at a rate faster than that of groundwater in the spring vent (Gulley et al., 2011; Brown et al., 2014). Due to the influence of rainfall events and the river water backflow into spring vent, not all the spring discharge data are suitable for analyzing the recession curve of karst spring hydrograph. Therefore, this study selects two recession periods of spring discharge, for which the influence of rainfall and river water backflow is small. The two periods are marked in Fig. 5, and more details of the two recession periods are given in Table 1. The two periods have different characteristics. The first period has a shorter period and smaller spring discharge in comparison with the second period. In addition, the amount of cumulative precipitation 30 days

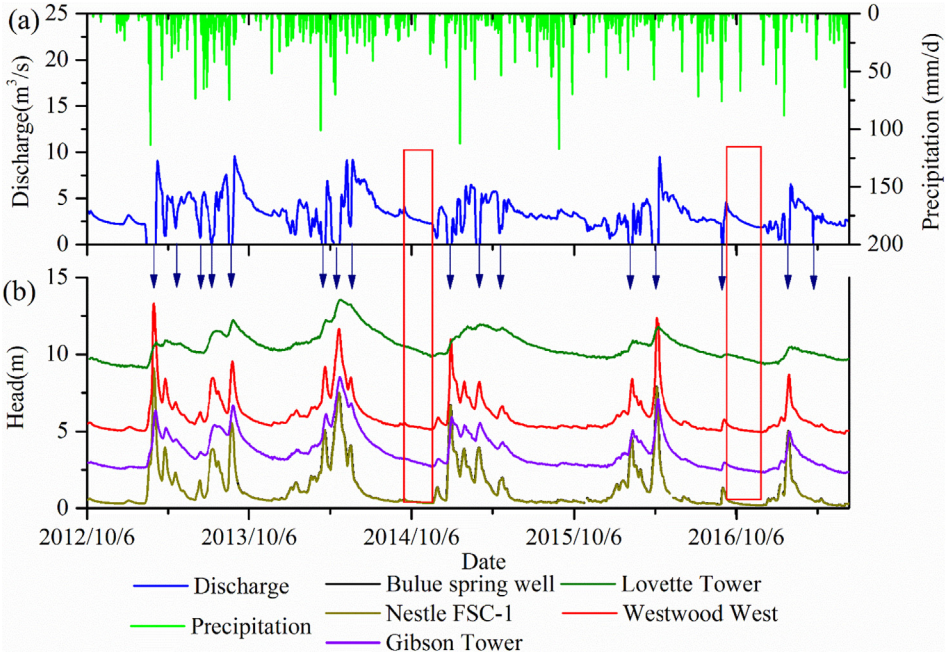

Fig. 5. (a) Precipitations and spring discharges from Oct. 06, 2012 to June 6, 2017. (b) Observation well head data in meters above spring outlet. The arrow keys represent water flow from the spring reversed into the conduits. The data resources are SRWMD (2017a,b) and USGS (2017).

Table 1
Starting dates and durations of two selected recession periods of karst spring hydrograph, and the maximum, minimum, and average spring discharge of the two periods. The cumulative precipitations are calculated for 30 days before the starting dates of the two periods.

	Starting Date	Duration (day)	Q_{max} (m^3/s)	Q_{min} (m^3/s)	Q_{mean} (m^3/s)	Cumulative precipitation (mm)
Recession Period 1	9/20/2014	25	4.08	2.71	3.09	122.39
Recession Period 2	9/13/2016	82	4.59	1.85	2.58	238.51

before the first period is smaller than that before the second period. The characteristic data of the two periods suggests that the conduit flow in the first period is smaller than that in the second period.

4. Results and discussion

Section 4.1 presents the results of simulating the observed data of spring discharge using the new model, the Mangin model, and the Fiorillo model, followed by a comparison of the simulation results of the three models in Section 4.2. The results of estimating groundwater discharge from the matrix and conduit reservoir and of estimating effective porosity of the matrix and conduit reservoirs of the three stages are given in Section 4.3. In Section 4.4, the estimated effective porosity of the matrix reservoir is compared with measured matrix porosity along two wells at the study site.

4.1. Simulated spring discharge

Fig. 6 plots the measured and calculated spring discharge by using the new model with one conduit layer, the new model with two conduit layers, the Mangin model, and the Fiorillo model. The fitted equations of the three models are listed in Table 2. The reason of considering the two options of using one conduit layer and two conduit layers for the new model during the mixed-drainage stage is to investigate to what extent the use of multiple conduit layers to represent different levels of karstification in the conduit reservoir can improve the simulation of measured spring discharge. In Fig. 6a and b for the new model with one conduit layer, the two vertical dashed lines in red separate the karst spring hydrograph into the conduit-drainage stage, the mixed-drainage stage, and the matrix-drainage stage. In Fig. 6c and d for the new model with two conduit layers, the vertical dashed lines in blue further separate the mixed-drainage stage into two sub-stages corresponding to the discharge from the two conduit layers. Comparing Fig. 6a–b with Fig. 6c–d shows that using two conduit layers improves the simulation of the measured spring hydrograph (especially for the second recession period plotted in Fig. 6b and d), and the improvement is quantified below using the misfit defined in Eq. (13).

In Fig. 6a–d, for the mixed-drainage stage, the simulated matrix flow and conduit flow are plotted separately. While the matrix flow varies slightly over time, the conduit flow has a large variation, especially for the second recession period plotted in Fig. 6b and d. While the conduit flow is substantially smaller than the matrix flow in Fig. 6a and c, the conduit flow is comparable with the matrix flow (especially in the early time of the mixed-drainage stage) in Fig. 6b and d. Therefore, it is necessary to separate conduit flow and matrix flow for the second recession period shown in Fig. 6b and d.

Fig. 6e and f plot the measured and calculated spring discharge by using the Mangin model for the two recession periods. In each figure, the vertical dashed line separates the fast flow ($\psi(t)$ from the unsaturated zone) and the slow flow ($\varphi(t)$ from the saturated zone) (Fig. 3a); $\psi(t)$ becomes zero in the period when spring discharge is only from slow flow (i.e., in the periods after the vertical lines). While the fitting between the measured and calculated spring discharge is satisfactory in Fig. 6e, the fitting is less satisfactory in Fig. 6f, especially in the early time when the quick flow is significant. The reason is that the simulated slow flow in the early time is relatively large. This problem cannot be resolved in the Mangin model, because it conceptualizes that slow flow from saturated zone always contributes to spring discharge during the entire recession period.

Fig. 6g and h plot the measured and calculated spring discharge by using the Fiorillo model for the two recession periods. In each figure, the vertical dashed lines separate the hydrograph into three periods

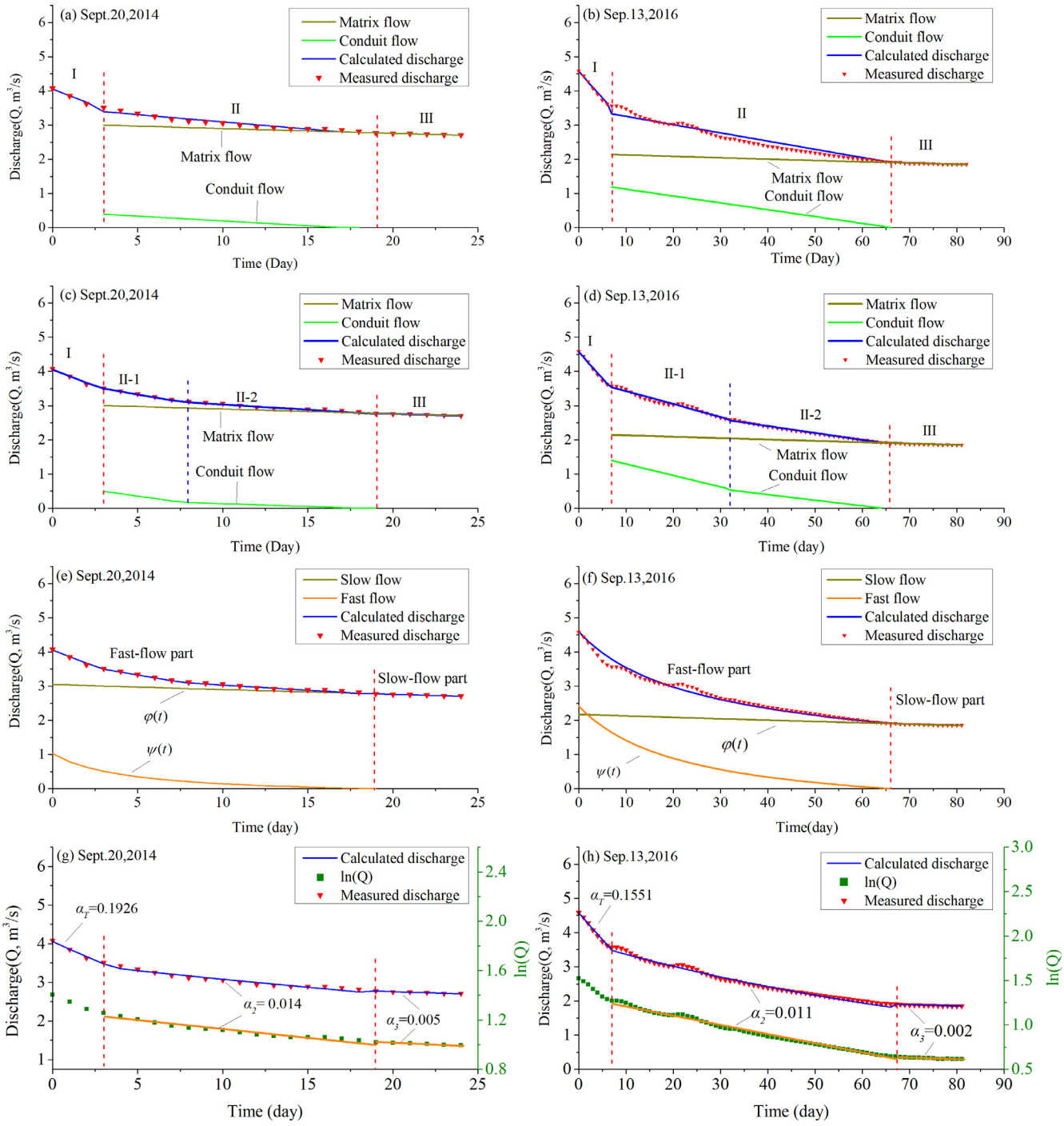

Fig. 6. Measured and calculated spring discharge using (a-b) the new model with only one conduit layer, (c-d) the new model with two conduit layers, (e-f) the Mangin model, and (g-h) the Fiorillo model. The left and right columns are for the recession periods starting on September 20, 2014 and September 13, 2016, respectively. Semi-logarithm plots ($\ln(Q) \sim t$) are shown in Figures (g-h) to demonstrate the linear relation between $\ln(Q)$ and t.

representing spring discharge from three tanks (Fig. 3b). The flow in the first period is the spring discharge from the tank that represents conduits, and the flows in the other two periods are the spring discharge from the tanks that represent fracture and matrix. While the fitting between the measured and calculated spring discharge is satisfactory in Fig. 6g, the fitting is less satisfactory in Fig. 6h in the second period when both matrix flow and conduit flow contribute to the spring discharge. To demonstrate the linear relation between the logarithm of discharge ($\ln Q$) and time (t) in the latter two flow periods, Fig. 6g and h plot the relation of $\ln Q \sim t$ for the two periods, and the linear relation is observed.

4.2. Comparison between the new model and the other two models

Fig. 7 plots the residuals (differences between observed and simulated spring discharge) of the four model simulations for the two recession periods. The misfit (i.e., the sum of absolute residuals as defined in Eq. (13)) is the largest for the new model with only one conduit layer (denoted as New Model-1 in Fig. 7), and the misfit is significantly larger than those of the other three simulations. These indicate that it is necessary to separate the conduit reservoir into two conduit layers in the mixed-drainage stage.

For the first recession period (Fig. 7a), the misfit of the new model

Table 2
Fitted equations for the new model (with only one conduit layer and two conduit layers), the Mangin model, and the Fiorillo model for the two recession periods listed in Table 1.

Model			Recession Period 1	Recession Period 2
New Model	Stage I		$Q_t = 4.06 - 0.193\,t\ (0 \le t < 3)$	$Q_t = 4.57 - 0.155\,t\ (0 \le t < 7)$
	One layer	Stage II	$Q_t = [0.39 - 0.028(t-3)] + 3.0e^{-0.005(t-3)}\ (3 \le t < 19)$	$Q_t = [1.19 - 0.02(t-7)] + 2.14e^{-0.002(t-7)}\ (7 \le t < 66)$
	Two layers	Stage II-1	$Q_t = [0.51 - 0.070(t-3)] + 3.0e^{-0.005(t-3)}\ (3 \le t < 7)$	$Q_t = [0.034 - 0.034(t-7)] + 2.14e^{-0.002(t-7)}\ (7 \le t < 32)$
		Stage II-2	$Q_t = [0.20 - 0.016(t-7)] + 3.0e^{-0.005(t-3)}\ (7 \le t < 19)$	$Q_t = [0.53 - 0.017(t-32)] + 2.14e^{-0.002(t-7)}\ (32 \le t < 66)$
	Stage III		$Q_t = 2.77e^{-0.005(t-19)}\ (t \ge 19)$	$Q_t = 1.91e^{-0.002(t-66)}\ (t \ge 66)$
Mangin Model			$\psi(t) = 1.03\frac{1-0.053t}{1+0.262t}\ (0 \le t \le 19)$ $\varphi(t) = 3.05e^{-0.005t}\ (t \ge 0)$	$\psi(t) = 2.41\frac{1-0.015t}{1+0.045t}\ (0 \le t \le 66)$ $\varphi(t) = 2.17e^{-0.002t}\ (t \ge 0)$
Fiorillo Model			$Q_t = 4.06–0.193\,t\ (0 \le t < 3)$ $Q_t = 3.40e^{-0.014(t-3)}\ (3 \le t < 19)$ $Q_t = 2.77e^{-0.005(t-19)}\ (t \ge 19)$	$Q_t = 4.57–0.155\,t\ (0 \le t < 7)$ $Q_t = 3.48e^{-0.011(t-7)}\ (7 \le t < 66)$ $Q_t = 1.91e^{-0.002(t-66)}\ (t \ge 66)$

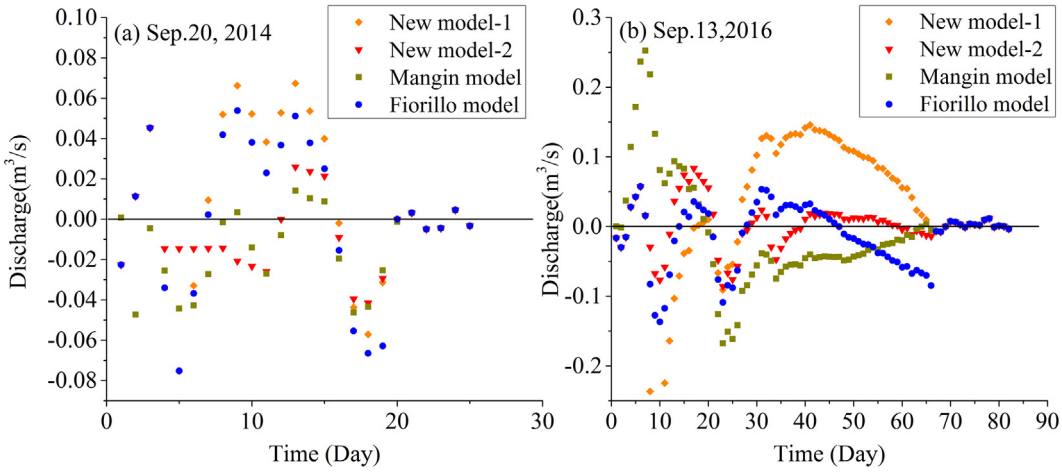

Fig. 7. Residuals between observed and calculated spring discharge of the three models for (a) the first recession period starting on 2014/9/20 and (b) the second recession period starting on 2016/9/13.

with two conduit layers (denoted as New Model-2 in Fig. 7) is 0.433, which only slightly smaller than the misfit of 0.436 m^3/s for the Mangin model and the misfit of 0.447 m^3/s for the Fiorillo model. This is not surprising, because the simulations of the three models fit the observations almost equally well, as shown in Fig. 6. This is attributed to the large matrix flow during the recession period, which can be simulated by all the three models. In other words, the mixed-drainage stage of the new model is essentially a matrix-drainage stage, and the separation of conduit flow and matrix flow in the mixed-flow period does not improve the goodness-of-fit of the new model.

For the second recession period (Fig. 7b) when the conduit flow is substantial during the mixed-flow period, the new model with two conduits layers and the Fiorillo model outperform the Mangin model, and the new model with two conduit layers outperforms the Fiorillo model. This is evidenced by the calculated misfit values, which are 1.895, 4.286, and 2.747 m^3/s for the new model with two conduit layers, the Mangin model, and the Fiorillo model, respectively. The reason that the new model with two conduit layers and the Fiorillo model outperform the Mangin model is that the Mangin model assumes that both conduit flow (unsaturated flow) and matrix flow (saturated flow) contribute to the fast flow (unsaturated flow). In other words, the Mangin model overestimates the early spring hydrograph, because the model assumes that matrix flow occurs during the entire recession period, as shown in Fig. 6f.

There are two reasons that the results of the new model with two conduit layers are better than those of this study's implementation of the Fiorillo model. One reason is that the new model separates matrix flow and conduit flow during the mixed-drainage stage, considering that the two models use the same equations for the conduit-drainage stage and the matrix-drainage stage (Table 2). The other reason is that the new model uses two conduit layers to represent different levels of karstification. The latter reason is more important than the former reason, which is self-evident because the new model with only one conduit layer cannot satisfactorily simulate the measured spring discharge. The new model has the following two flexibilities: (1) since the new model separates the mixed flow into conduit flow and matrix flow, it can use the linear equation and the exponential model for simulating conduit flow and matrix flow, respectively; (2) since the new model considers multiple conduit layers, it can uses multiple linear equations to simulate the variation of conduit flow, which may be caused by hydraulic head differences between the matrix and conduit reservoirs as observed at the Aumelas-Thau karst system in France and the Santa Fe karst system in Florida (Bailly-Comte et al., 2010) These flexibilities are not available in this study's implementation of the Fiorillo model. It is possible that using multiple exponential equations during the mixed-flow period may improve the results of the Fiorillo model.

4.3. Estimated discharge volume and effective porosity

Table 3 lists the estimated effective porosity for the two recession periods; the table also lists the estimated discharge volumes and head ranges needed for the porosity estimation. The head ranges are listed in the format of heads at the beginning and ending time of each drainage stage. For example, the range of 6.06 m–5.93 m corresponds to $h_{1,m}$–$h_{2,m}$, the matrix heads of the beginning and ending time of the mixed-drainage stage for recession period 1. The drainage area, A_c, needed for the porosity estimation takes the value of 259 km^2 (SRWMD, 2004b). The average hydraulic head, $h_{2,c}$, takes the value of 0.16 m, the

Table 3
Ranges of estimate hydraulic head, discharge volumes, and estimates of effective porosity related to the matrix reservoir and two conduit layers.

	Head range (m)		Discharge volume (m^3)		Effective porosity (%)		
	Matrix	Conduits	Matrix	Conduit	Matrix	Conduit	Total
Recession Period 1							
Stage I	/	8.24–6.06	0	976,303	/	0.17	/
Stage II	6.06–5.93	6.06–1.26	4,009,181	127,227	11.91	0.010	11.94
		1.26–0.16		117,461		0.041	
Stage III	5.93–5.89	/	1,182,744	0	11.42	/	/
Recession Period 2							
Stage I	/	9.46–5.72	0	2,436,104	/	0.25	/
Stage II	5.72–5.36	5.72–0.97	10,306,007	2,103,438	11.37	0.17	11.64
		0.97–0.16		779,594		0.37	
Stage III	5.36–5.28	/	2,431,959	0	11.74	/	/

lowest hydraulic head at the monitored wells. The impacts of the assumed $h_{2,c}$ value are discussed below.

The table suggests that, for the two recession periods, while hydraulic head in the matrix decreases slightly (from 6.06 m to 5.89 m in the first recession period and from 5.72 m to 5.28 m in the second recession period), hydraulic head in the conduit reservoir decreases substantially (from 8.24 m to 0.16 m in the first recession period and from 9.46 m to 0.16 m in the second recession period). The head variations indicate that the conduit flow is more dynamics than the matrix flow. As a result, the estimation of matrix porosity is more stable than the estimate of conduit porosity, as discussed below.

For the two recession periods, groundwater discharge from the matrix reservoir is substantially larger than that from the conduit reservoir. For the first recession period, the groundwater discharges from the matrix and conduit reservoirs are 5,191,925 m^3 and 1,220,991 m^3, respectively. For the second recession period, the groundwater discharges from the matrix and conduit reservoirs increase to 12,737,966 m^3 and 5,319,136 m^3, respectively. It is expected that the groundwater discharge from the matrix reservoir is larger than that from the conduit reservoir, considering that the estimated matrix flow is substantially larger than the estimated conduit flow in this study area (Fig. 6c and d). The increase of groundwater discharge in the second recession period is reasonable, considering that the precipitation before the second recession period is about twice as large as the precipitation before the first recession period (Table 1). Therefore, the estimated values of matrix and conduit porosity of the second recession period should better reflect the karst system than those of the first recession period.

Table 3 indicates that, while the estimated matrix porosity is consistent for the two recession periods, the estimated conduit porosity varies substantially between the two recession periods. For example, the estimated conduit porosity of the mixed-drainage stage in the first recession period is about one order of magnitude smaller than those in the second recession period. The estimated conduit porosity of the second recession period should be more reasonable than that of the first recession period, because the conduit flow of the second recession period is substantially larger than that of the first recession period (Fig. 6d). In other words, the conduit reservoir is filled with more water in the second recession period than in the first recession period.

Since the value of conduit head, $h_{2,c}$, is assumed to be 0.16 m, it is necessary to evaluate the impact of the assumed value on the estimation of effective conduit porosity. Fig. 8 plots the variation of estimated conduit porosity of the two conduit layers for a number of $h_{2,c}$ values between 0.16 m and 1 m, which was used by **Li et al. (2013, 2016) for studying the hydrograph of the St. Marks Spring that is close to the Madison Blue Spring. The figure shows that the impact is small for conduit layer 1 in terms of the absolute difference. For example, when the conduit head ($h_{2,c}$) increases from 0.16 m to 1 m, the estimated effective porosity increases from 0.010% to 0.012% for the first recession period and from 0.17% to 0.20% for the second recession period. The absolute increase is larger for conduit layer 2, which is from 0.041% to 0.048% for the first recession period and from 0.37% to 0.44% for the second recession period. The larger impact on conduit layer 2 than on conduit layer 1 is reasonable, because conduit layer 2 is closer to the conduit vent than conduit layer 1 is. When the relative increase of effective conduit porosity is calculated for the two conduit layers and the two recession periods, the relative increase is about 20%, which is significant. Therefore, it is necessary to have a reasonable estimation of conduit head, $h_{2,c}$.

4.4. Evaluation of estimated effective porosity

The estimated effective porosity of the matrix reservoir is evaluated by comparing the estimated porosity with the measured (from rock samples) matrix porosity at two wells, W-15515 and W-15537, completed in 1984 in the study area (Hoenstine, 1990; Upchurch, 2004). Fig. 9 shows the vertical profiles of measured matrix porosity along the two wells. While the measured matrix porosity varies substantially with depth, the average matrix porosity is about 12% for the two wells, close to the estimated values listed in Table 3. It suggests that the estimated effective porosity of the matrix reservoir is reasonable. Since the estimated matrix porosity is not for the entire aquifer but for the portion of the aquifer where matrix head varies during the recession periods, we calculate the average matrix porosity for the intervals where matrix head varies. For the two wells, the intervals were marked by the grey boxes based on the measured head of Upchurch (2004) and CHoenstine (1990)***. The average matrix porosity is 13.5% for well 15,515 and 10.5% for well 15537. These average values bracket the estimated matrix porosity listed in Table 3, suggesting that the estimated matrix porosity is reasonable. It should be noted that the matrix porosity of the Floridan aquifer can be as high as 30% (Budd and Vacher, 2004; Peterson and Wicks, 2005).

Since on-site measurements of conduit porosity are not available, the estimated effective porosity values of conduit reservoirs (listed in Table 3) are compared with literature data. The estimated values are comparable with the estimate channel porosity values listed in Worthington (1999) and Worthington et al. (2000), which are 0.003% for Smithville, Ontario, Canada, 0.06% for Mammoth Cave, Kentucky, USA, 0.02% for the Chalk, England, and 0.5% for Nohoch Nah Chich, Yucatan, Mexico. Except the low value of 0.003%, the literature values are of the same order of magnitude with those listed in Table 3 at different drainage stages. The matrix porosity and channel porosity specific to the Cenozoic limestone at Yucatan are of particular interest, due to similar geology between Yucatan and Florida. The estimated matrix porosity of the Yucatan limestone is 17%, about 42% larger than the estimate of 12% in this study; the estimated channel porosity of the Yucatan limestone is 0.5%, about 35% larger than the largest estimate of 0.37 in this study. This different is not unreasonable, because the site

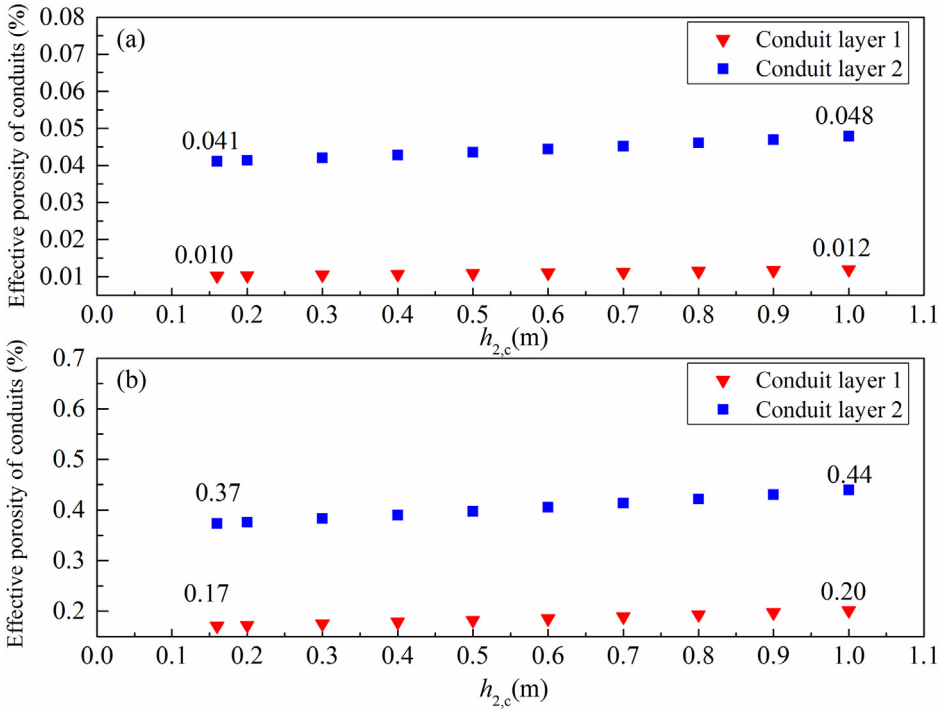

Fig. 8. Variation of estimated effective porosity of two conduit layers with the conduit head ($h_{2,c}$) for (a) the first recession period starting on 9/20/2014 and (b) the second recession period starting on 9/13/2016.

area of this study is supposed to be smaller than that of the Yucatan limestone.

Worthington (1999) and Worthington et al. (2000) also listed the proportion of aquifer storage in matrix, fracture, and channel, which are 99.7% for Smithville, 96.4% for Mammoth Cave, 99.9% for the Chalk, and 96.6% for Nohoch Nah Chich. The matrix storage is conceptually similar to the matrix flow in this study (although not the same), and Table 3 indicates that the matrix storage is about 97% for recession period 1 and 83–92% for recession period 2. This suggests that the estimated amount of flow and the estimated reservoir porosity are comparable to those reported in literature. However, it should be noted that the comparison is qualitative only, and caution should be taken. For example, in Worthington et al. (2000), channel is referred to as "all interconnected disolutional enlargements along joints, faults, and bedding planes". This definition is certainly broader than the concept of conduit reservoir used in this study.

5. Conclusions

This paper presents a new model for simulating karst spring recession curves. The new model has the following three characteristics: (1) the model considers two separate but hydraulically connected reservoirs: matrix reservoir and conduit reservoir; (2) the model separates a recession period of a karst spring hydrograph into three drainage stages: conduit-drainage stage (with only conduit flow in conduits), mixed-drainage stage (with both conduit flow in conduits and matrix flow from matrix to conduits), and matrix-drainage stage (with only matrix flow from matrix to conduits); and (3) in the mixed-drainage stage, the model uses multiple conduit layers to present different levels of conduit development. The new model is conceptually similar to the

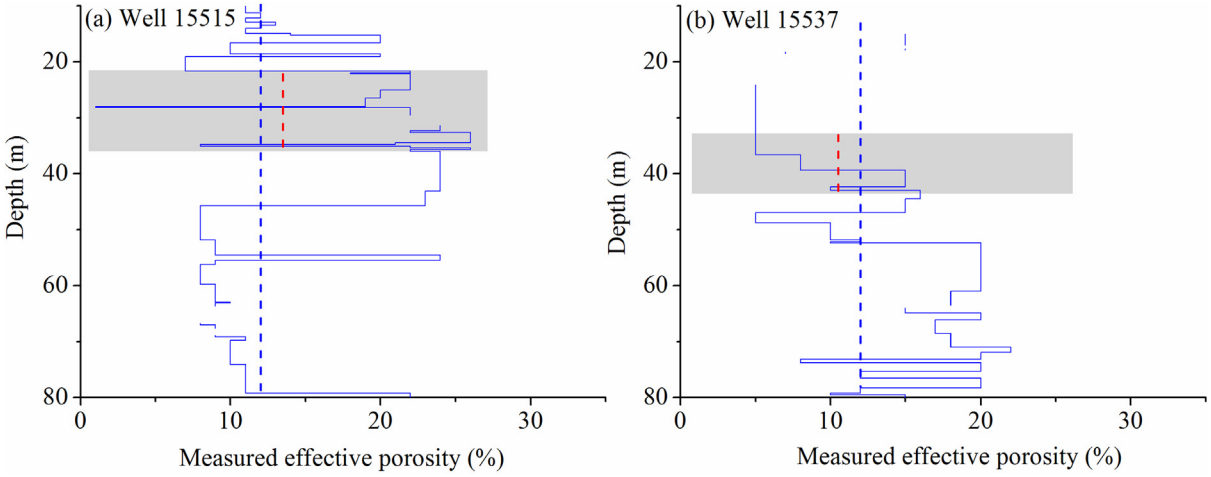

Fig. 9. Vertical profiles of measured matrix porosity along (a) well 15,537 and (b) well 15,515 drilled in the study area. The dashed blue lines represent the average porosity along the entire profiles, and the dashed red lines represent the average porosity for the grey areas that mark matrix head variation. (For interpretation of the references to colour in this figure legend, the reader is referred to the web version of this article.)

Fiorillo model, but has two unique features for handling the mixed-drainage stage, i.e., explicitly separating conduit flow and matrix flow and using multiple conduit layers to represent different levels of karst development.

When using the new model, the Mangin model, and the Fiorillo model for simulating the observed spring discharge at the Madison Blue Spring, the new model and the Fiorillo model outperform the Mangin model, because the Mangin model assumes continuous matrix flow from the beginning of the recession and thus overestimates the early spring discharge. Due to the flexibilities of using linear equation and exponential equation to simulate conduit flow and matrix flow, respectively, and of using multiple conduit layers for the mixed-drainage stage, the results of the new model are better than those of this study's implementation of Fiorillo model. The results of the Fiorillo model may be improved by using multiple exponential functions, and this exploration is warranted in future studies.

Based on the new model of simulating the recession curves of karst spring hydrograph, the groundwater discharge volumes from the matrix and conduit reservoirs are estimated. The results indicate that the discharge from the matrix reservoir is substantially larger than the discharge from the conduit reservoir, especially in the first recession period when conduit flow is smaller than the second recession period. As a result, the estimated effective porosity of the conduit reservoir for the second recession period better characterize the conduit reservoir than that for the first recession period. While there is lacking field measurements to evaluate the estimated effective porosity of the conduit reservoir, the estimated effective porosity of the matrix reservoir agrees with the porosity values measured from borehole samples at the study site.The new model of simulating the recession curves of karst spring hydrograph has four limitations. The first limitation is that the new model requires a relatively long recession period until the matrix-drainage stage appears on the karst spring hydrograph. The requirement for a relatively long recession period is resulted from the procedure of hydrograph separation, i.e., Steps (3) and (4) described in Section 2.1. Specifically speaking, the recession coefficient, α_2, is first estimated for the matrix-drainage stage, and its value is assumed for the recession coefficient, α_1, for simulating the matrix flow of the mixed-drainage stage. The long recession periods may not occur often for areas (e.g., Florida) with frequent rainfall events. This limits the applicability of the new model for simulating karst spring hydrograph and for characterizing karst aquifers. The second limitation is that the estimation of effective porosity of matrix and conduit reservoirs requires knowing the springshed area (A_c) and the conduit hydraulic head ($h_{2,c}$) at the end of the mixed-drainage stage. While the area (A_c) can be estimated based on available hydrologic information, the area is assumed to be a constant over time, which may not be realistic, especially when hydrologic conditions change dramatically over time in Florida. In addition, the estimated springshed does not consider groundwater flow from adjacent springsheds, and karst spring hydrograph may only represent a fraction of the springshed. For conduit head, $h_{2,c}$, it cannot be directly estimated because measurements of conduit head are always lacking. The third limitation is that the new model is only applicable to unconfined karst aquifers, for which the karst spring recession curve can reflect the internal structure and properties of the karst aquifers. For example, the effective porosities defined in this study are only applicable to unconfined karst aquifers, because head variation of confined aquifers does not reflect the volumes of matrix and conduit reservoirs. The last limitation of this research is that it cannot provide a systematic way of evaluating the estimated conduit porosity. Since there is always lacking of measurements of conduit porosity, it is necessary to evaluate the estimated conduit porosity using other approaches. One of the approaches is the hydrochemical model of de Rooij and Graham (2017) that can explicitly characterize karst conduit networks and estimate conduit porosity. Worthington (2015) provided more insights on karst conduit formation and its characterization from the hydrogeological perspective. Future research is warranted for linking this research, which is statistical in nature, with other theoretical researches for better characterizing conduits of karst aquifers.

Acknowledgements

This research was supported in part by the National Key R&D Program of China (Grant 2017YFC0804102). The first author was supported by the China Scholarship Council for his research in the Department of Scientific Computing at the Florida State University. The second author was supported by National Science Foundation grant, EAR-1828827.

References

Arthur, J.D., Baker, A.E., Cichon, J.R., Wood, A.R., Rudin, A., 2005. Florida Aquifer Vulnerability Assessment (FAVA): Contamination potential of Florida's principal aquifer systems. Report submitted to the Division of Water Resource Management, Florida Department of Environmental Protection. Tallahassee: Division of Resource Assessment and Management, Florida Geological Survey, 156 pp.

Bailly-Comte, V., Martin, J.B., Jourde, H., Screaton, E.J., Séverin, P., Abigail, L., 2010. Water exchange and pressure transfer between conduits and matrix and their influence on hydrodynamics of two karst aquifers with sinking streams. J. Hydrol. 386 (1), 55–66.

Bonacci, O., 1993. Karst springs hydrographs as indicators of karst aquifers. Hydrol. Sci. J. 38 (1), 51–62. http://dx.doi.org/10.1080/02626669309492639.

Boussinesq, J., 1877. Essai sur la théorie des eaux courantes do mouvement non permanent des eaux souterraines. Acad. Sci. Inst. Fr. 23, 252–260.

Boussinesq, J., 1904. Recherches théoriques sur l'écoulement des nappes d'eau infiltrées dans le sol et sur le débit des sources. Journal de mathématiques pures et appliquées 10, 5–78.

Brown, A.L., Martin, J.B., Screaton, E.J., Ezell, J.E., Spellman, P., Gulley, J., 2014. Bank storage in karst aquifers: the impact of temporary intrusion of river water on carbonate dissolution and trace metal mobility. Chem. Geol. 385, 56–69. http://dx.doi.org/10.1016/j.chemgeo.2014.06.015.

Budd, D.A., Vacher, H.L., 2004. Matrix permeability of the confined Floridan Aquifer, Florida USA. Hydrogeol. J. 12 (5), 531–549.

Bush, P.W., Johnston, R.H., 1988. Ground-water hydraulics, regional flow, and groundwater development of the Floridan aquifer system in Florida and in parts of Georgia, South Carolina, and Alabama. 2330–7102, US Government Printing Office, 89 pp.

Chang, Y., Wu, J., Liu, L., 2015. Effects of the conduit network on the spring hydrograph of the karst aquifer. J. Hydrol. 527, 517–530. http://dx.doi.org/10.1016/j.jhydrol.2015.05.006.

Copeland, R.E., 2003. In: Florida Spring Classification System and Spring Glossary. Florida Geological Survey. Special Publication No. 52, pp. 22.

de Rooij, R., Graham, W., 2017. Generation of complex karstic conduit networks with a hydrochemical model. Water Resour. Res. 53, 6993–7011.

Dewandel, B., Lachassagne, P., Bakalowicz, M., Weng, P., Al-Malki, A., 2003. Evaluation of aquifer thickness by analysing recession hydrographs. Application to the Oman ophiolite hard-rock aquifer. J. Hydrol. 274 (1–4), 248–269. http://dx.doi.org/10.1016/s0022-1694(02)00418-3.

Draper, N.R., Smith, H., 1998. Applied Regression Analysis. Wiley University of Michigan.

Fiorillo, F., 2009. Spring hydrographs as indicators of droughts in a karst environment. J. Hydrol. 373 (3–4), 290–301. http://dx.doi.org/10.1016/j.jhydrol.2009.04.034.

Fiorillo, F., 2011. Tank-reservoir drainage as a simulation of the recession limb of karst spring hydrographs. Hydrogeol. J. 19 (5), 1009–1019. http://dx.doi.org/10.1007/s10040 -011-0737-y.

Fiorillo, F., 2014. The recession of spring hydrographs, focused on karst aquifers. Water Resour. Manage. 28 (7), 1781–1805. http://dx.doi.org/10.1007/s11269-014-0597-z.

Ford, D., Williams, P.D., 2013. In: Karst Hydrogeology and Geomorphology. John Wiley & Sons, pp. 576.

Fu, T., Chen, H., Wang, K., 2016. Structure and water storage capacity of a small karst aquifer based on stream discharge in southwest China. J. Hydrol. 534, 50–62. http://dx.doi.org/10.1016/j.jhydrol.2015.12.042.

Geyer, T., Birk, S., Liedl, R., Sauter, M., 2008. Quantification of temporal distribution of recharge in karst systems from spring hydrographs. J. Hydrol. 348 (3–4), 452–463. http://dx.doi.org/10.1016/j.jhydrol.2007.10.015.

Ghasemizadeh, R., Hellweger, F., Butscher, C., Padilla, I., Vesper, D., Field, M., Alshawabkeh, A., 2012. Review: groundwater flow and transport modeling of karst aquifers, with particular reference to the North Coast Limestone aquifer system of Puerto Rico. Hydrogeol. J. 20 (8), 1441–1461. http://dx.doi.org/10.1007/s10040-012-0897-4.

Goldscheider, N., Drew, D. (Eds.), 2007. Methods in Karst Hydrogeology. International Contribution to Hydrogeology, IAH. Taylor and Francis/Balkema, London, pp. 279.

Goldscheider, N., 2015. Overview of methods applied in karst hydrogeology. Karst Aquifers—Characterization and Engineering, 127–145.

Greenhalgh, T., 2003. In: Florida First Magnitude Springsheds. Florida Geological Survey, Tallahassee, FL, pp. 12.

Grubbs, J., 1998. Recharge rates to the upper Floridan Aquifer in the Suwannee River Water Management District, Florida, US Dept. of the Interior, US Geological Survey, 36 pp.

Gulley, J., Martin, J.B., Screaton, E.J., Moore, P.J., 2011. River reversals into karst

springs: a model for cave enlargement in eogenetic karst aquifers. Geol. Soc. Am. Bull. 123 (3–4), 457–467.
Gupta, R.S., 2016. Hydrology and Hydraulic Systems. Waveland Press Inc., Long Grove, IL, pp. 888.
Hoenstine, R.W., Steven M., Spencer, O'Carroll, Teresa, 1990. Geology and ground-water resources of Madison County, Florida, 114 pp.
Kiraly, L., 2003. Karstification and groundwater flow. Speleogenesis Evol. Karst Aquifers 1 (3), 155–192.
Kovács, A., 2003. Geometry and hydraulic parameters of karst aquifers. Thèse de doctorat Thesis Thesis, Université de Neuchâtel, 134 pp.
Kovács, A., Perrochet, P., 2008. A quantitative approach to spring hydrograph decomposition. J. Hydrol. 352 (1–2), 16–29. http://dx.doi.org/10.1016/j.jhydrol.2007.12.009.
Kovács, A., Perrochet, P., Király, L., Jeannin, P.Y., 2005. A quantitative method for the characterisation of karst aquifers based on spring hydrograph analysis. J. Hydrol. 303 (1–4), 152–164. http://dx.doi.org/10.1016/j.jhydrol.2004.08.023.
Kullman, E., 1990. Krasovo-puklinové vody (Karst-issure waters; in Slovak). Geologický ústav Dionýza Štúra, Bratislava, pp. 184.
Li, G., Field, M.S., 2013. A mathematical model for simulating spring discharge and estimating sinkhole porosity in a karst watershed. Grundwasser 19 (1), 51–60. http://dx.doi.org/10.1007/s00767-013-0243-3.
Li, G., Goldscheider, N., Field, M.S., 2016. Modeling karst spring hydrograph recession based on head drop at sinkholes. J. Hydrol. 542, 820–827. http://dx.doi.org/10.1016/j. jhydrol.2016.09.052.
Maillet, E.T., 1905. Essais d'hydraulique souterraine & fluviale. A. Hermann, Paris, 218 pp.
Malík, P., Vojtková, Silvia, 2012. Use of recession-curve analysis for estimation of karstification degree and its application in assessing overflow/underflow conditions in closely spaced karstic springs. Environ. Earth Sci. 65 (8), 2245–2257.
Martin, J.B., Dean, Randolph W., 2001. Exchange of water between conduits and matrix in the Floridan aquifer. Chem. Geol. 179 (1), 145–165. http://dx.doi.org/10.1016/S0009-2541(01)00320-5.
Martin, J.B., Screaton, E.J., 2001. Exchange of matrix and conduit water with examples from the Floridan aquifer. In: US Geological Survey Karst Interest Group Proceedings, Water-Resources Investigations Report, 1(4011), 38–44.
Mangin, A., 1975. Contribution à l'étude hydrodynamique des aquifères karstiques. 30(1), pp. 21–124.
Milanovic, P.T., 1981. Karst Hydrogeology. Water Resources Publications, Littleton, Colorado, USA, pp. 281.
National Center for Environmental Information (NOAA), 2017. Weather records from Madison station. https://www.ncdc.noaa.gov/cdo-web/datatools/findstation (last accessed June 18, 2017).
Peterson, E.W., Wicks, C.M., 2005. Fluid and solute transport from a conduit to the matrix in a carbonate aquifer system. Math. Geol. 37 (8), 851–867. http://dx.doi.org/10.1007/ s11004-005-9211-5.
Scott, T.M., 1988. The Lithostratigraphy of the Hawthorn Group (Miocene) of Florida: Florida. Bulletin 59, Florida Geological Survey, 148 pp.
Shevenell, L., 1996. Analysis of well hydrographs in a karst aquifer: estimates of specific yields and continuum transmissivities. J. Hydrol. 174 (3), 331–355. http://dx.doi.org/10.1016/0022-1694(95)02761-0.
Shoemaker, W.B., Kuniansky, E.L., Birk, S., Bauer, S., Swain, E.D., 2008. Documentation of a conduit flow process (CFP) for MODFLOW-2005, pp 58.
Suwannee River Water Management District (SRWMD), 2004a. Delineation of spring protection areas at five, first-magnitude springs in north-central Florida. Suwannee River Water Management District, pp 30.
Suwannee River Water Management District (SRWMD), 2004b. Development of Madison blue spring-based MFL, technical report. Suwannee River Water Management District, pp 236.
Suwannee River Water Management District (SRWMD), 2017a. Daily total rainfall from the following monitoring site: Madison Blue Springs, Madison Blue Springs weather station. http://www.mysuwanneeriver.org/portal/springs.htm (last accessed June 18, 2017).
Suwannee River Water Management District (SRWMD), 2017b. Groundwater Levels from the following monitoring sites: Blue Springs Well, Nestle FSC-1 (N011117015), Gibson Tower (N021035003), Westwood West (N021013001), Lovette Tower (N020822002). http://www.mysuwanneeriver.org/portal/ groundwater.htm (last accessed June 18, 2017).
Stevanovic, Z., Milanovic, S., Ristic, V., 2010. Supportive methods for assessing effective porosity and regulating karst aquifers acta carsologica. Acta Carsol. 39 (2), 313–329.
Stevanovic, Z., 2015. In: Karst Aquifers-Characterization and Engineering. Springer International Publishing Switzerland, pp. 698. http://dx.doi.org/10.1007/978-3-319-12850-4.
Szilagyi, J., 1999. On the use of semi-logarithmic plots for baseflow separation. Ground Water 37 (5), 660–662. http://dx.doi.org/10.1111/j.1745-6584.1999.tb01157.x.
Taylor, C.J., Greene, E.A., 2008. Hydrogeologic characterization and methods used in the investigation of karst hydrology. Field techniques for estimating water fluxes between surface water and ground water, edited by Rosenberry, DO and LaBaugh, JW, US Geological Survey, Reston, Virginia (EUA), pp. 71–114.
Upchurch, S.B., 2004. In: Development of Madison Blue Spring-Based MFL Technical Report. Water Resource Associates, Inc., pp. 236.
United States Geological Survey (USGS), 2017. National Water Information System Data, stations 02319302. https://maps.waterdata.usgs.gov/mapper/index.html?state =fl (last accessed June 18, 2017).
Worthington, S., Ford, D.C., Beddows, P.A., 2000. Porosity and permeability enhancement in unconfined carbonate aquifers as a result of solution. ISBN 978-1-57958-399-6 In: Klimchouk, A., Ford, D., Palmer, A., Dreybrodt, W. (Eds.), Speleogenesis: Evolution of Karst Aquifers. Cave Books, St Louis, pp. 463–471.
Worthington, S.R.H., 1999. A comprehensive strategy for understanding flow in carbonate aquifers. In: Palmer, A.N., Palmer, M.V., Sasowsky, I.D. (Eds.), Karst Modelling. Symposium Proceedings, Charlottesville. Karst Water Institute, Spec Publ, pp. 30–37.
Worthington, S.R.H., 2015. Characteristics of channel networks in unconfi ned carbonate aquifers. Geol. Soc. Am. Bull. 127 (5–6). http://dx.doi.org/10.1130/B31098.1.